

ISM STUDIES OF GRB 030329 WITH HIGH RESOLUTION SPECTROSCOPY *

CHRISTINA C. THÖNE ¹, JOCHEN GREINER, SANDRA SAVAGLIO
 Max-Planck-Institut für Extraterrestrische Physik, Giessenbachstraße, 85748 Garching, Germany

EMMANUËL JEHIN
 European Southern Observatory, Alonso de Cordova 3107, Vitacura, Santiago 19, Chile
Draft version 24. November 2006

ABSTRACT

We present a series of early UVES/VLT high resolution spectra of the afterglow of GRB 030329 at redshift $z = 0.16867 \pm 0.00001$. In contrast to other spectra from this burst, both emission and absorption lines were detected. None of them showed any temporal evolution. From the emission lines, we determine the properties of the host galaxy which has a star formation rate (SFR) of $0.198 M_{\odot} \text{ yr}^{-1}$ and a low metallicity of $1/7 Z_{\odot}$. Given the low total stellar host mass $M_{\star} = 10^{7.75 \pm 0.15} M_{\odot}$ and an absolute luminosity $m_V = -16.37$, we derive specific SFRs (SSFR) of $\log \text{SFR}/M = -8.5 \text{ yr}^{-1}$ and $\text{SFR}/L = 14.1 M_{\odot} \text{ yr}^{-1} L_{\star}^{-1}$. This fits well into the picture of GRB hosts as being low mass, low metallicity, actively star forming galaxies.

The Mg II and Mg I absorption lines from the host show multiple narrow (Doppler width $b = 5\text{--}10 \text{ km/s}$) components spanning a range of $v \sim 260 \text{ km/s}$, mainly blueshifted compared to the redshift from the emission lines. These components are likely probing outflowing material of the host galaxy, which could arise from former galactic superwinds, driven by supernovae from star forming regions. Similar features have been observed in QSO spectra. The outflowing material is mainly neutral with high column densities of $\log N(\text{Mg II}) = 14.0 \pm 0.1 \text{ cm}^{-2}$ and $\log N(\text{Mg I}) = 12.3 \pm 0.1 \text{ cm}^{-2}$.

Subject headings: Gamma-rays: Bursts: Individual: GRB 030329, GRB host galaxies, absorption line kinematics, high resolution spectra

1. INTRODUCTION

Gamma-Ray-Bursts (GRBs) have proven to be one of the lighthouses in the distant universe since the determination of their cosmological origin in 1997 (van Paradijs et al. 1997; Metzger et al. 1997). Their afterglow spectra, ranging from X-ray to radio, follow a power law decay and do not seem to show intrinsic lines from the burst itself though there are some claims of X-ray line detections from the prompt emission (e.g., Butler et al. 2005, and references therein). This makes them well suited as a powerful light source to study the burst environment in the host galaxy and the medium in the line of sight by using absorption lines. In addition, emission lines from the host might be seen on top of the afterglow spectrum and provide important information about the type of galaxy in which GRBs occur. As these galaxies are usually very faint and difficult to detect, GRBs offer a unique possibility to find and study these galaxies in detail.

One of the few other possibilities to study these faint, distant galaxies is through QSO observations (Ellison et al. 2003; Petitjean et al. 2000). Their spectra often show intervening absorption systems from foreground damped Lyman alpha systems (DLAs) or metal absorption lines such as Mg II (Churchill et al. 2003) associated with galaxies or halos of galaxies. Mg II absorbers are the best studied sample to date as Mg II is

the reddest of the strong metal absorption lines in the interstellar medium (ISM), but also C IV, which probes a different region of the ISM has been studied since many years. Recently, highly excited lines like O VI have also been discovered in such absorption systems (Ellison et al. 2000; Schaye et al. 2000). With high resolution spectra, the stronger absorption lines of these QSO-absorbers usually have been found to consist of several components spanning velocities up to 300 km/s (Prochter et al. 2006). These different components are assumed to originate in different clouds in the absorbing system and are therefore able to give a picture of the ISM structure in these galaxies.

For an increasing fraction of GRBs, spectra of the afterglow can be obtained, especially since the *Swift* satellite (Gehrels et al. 2004) started operating in December 2004. Depending on the redshift and the wavelength range of the instrument, these spectra may contain emission lines from HII regions in the host galaxy or absorption lines from material inside the host galaxy and/or the intergalactic medium (IGM). Emission line analysis from the host galaxy can be easily performed with low resolution spectroscopy from the afterglow containing emission lines from the galaxy, or with later observations targeting the galaxy. These analyses reveal that host galaxies of long GRBs are usually young, irregular, low mass, low metallicity, star-forming galaxies (Christensen et al. 2004). To study the ISM structure in the host galaxy through absorption lines, however, higher resolution is needed which is only available for few bursts so far (Savaglio 2006, and references therein), most of them detected recently. Their absorption lines

*BASED ON ESO PROPOSAL 70.D-0087

Electronic address: cthoene@dark-cosmology.dk

¹ DARK Cosmology Centre, Niels-Bohr-Institut, Julianne Maries Vej 30, 2100 København Ø, Denmark

usually show several components with a wide range of velocities whose nature is still speculative. Due to the wavelength coverage of the spectra and the position of the absorption and emission lines, there are only very few bursts that contain both. Examples are GRB 990712 (Vreeswijk et al. 2004) and GRB 970508 (Reichart 1998) which had Mg II absorption in addition to the host emission lines. GRB 020813 (Barth et al. 2003) showed weak OII emission in addition to the broad absorption lines containing many velocity components and GRB 020405 (Masetti et al. 2003) had a weak Ca II absorption line. Only for one burst, GRB 060218 (Wiersema et al. 2006), high resolution spectra containing both kind of lines could be obtained which show different components in the host absorption and one of the emission lines.

The long GRB 030329 was detected by the HETE-2 satellite at 11:38:41 UT (Vanderspek et al. 2003) and lasted for $T_{90} = 22.9$ s at high energies. In terms of fluence, it was among the top 1% of all detected GRBs. A bright optical afterglow was detected 1.5 hr after the burst with an R-band magnitude of 12.5 (Peterson & Price 2003) allowing to get high resolution spectra. The optical lightcurve showed a slow decay with a power law index of $\alpha = -1.2 \pm 0.1$ and several phases of rebrightenings 1.3, 2.4, 3.1 and 4.9 days (Matheson et al. 2003; Lipkin et al. 2004) after the onset of the burst. From the emission lines of the host in the UVES spectra presented here, a redshift of $z=0.1685$ was determined (Greiner et al. 2003a).

Due to its brightness and low redshift, a series of low resolution spectra could be taken over several weeks, which showed for the first time the connection between long-duration GRBs and supernovae (SNe) (Hjorth et al. 2003; Matheson et al. 2003; Stanek et al. 2003). Also, for the first time, it was possible to measure the time evolution of the afterglow polarization (Greiner et al. 2003b). Emission line analysis of the host galaxy was obtained from an extensive low resolution dataset taken with the FORS spectrograph (Hjorth et al. 2003; Sollerman et al. 2005) and spectra from Matheson et al. (2003) who found a SFR of $0.5M_{\odot}/\text{yr}$ and a moderate metallicity of $12+\log(\text{O}/\text{H})=8.5$, but they assumed the upper branch of the metallicity solution. None of them however was able to detect any absorption line as the wavelength range of their spectra missed the Mg II lines in the UV.

In this paper, we present high resolution UVES/VLT spectra from the first and the fourth night after the burst. We detect and analyze both emission and absorption lines as shown in §3. The emission lines are used to derive the redshift, extinction, SFR and metallicity of the host galaxy in §4. §5 shows the splitting of the host absorption lines into 7 components and gives a possible interpretation of these components.

For the calculations in the paper, we used a $\Omega_{\Lambda} = 0.7$, $\Omega_m = 0.3$ cosmology, a value of $H=70$ km/s for the Hubble constant and $c=299,792$ km/s.

2. DATA SAMPLE

High-resolution spectra of the afterglow of GRB 030329 have been collected with the UV-Visual Echelle Spectrograph (UVES, Dekker et al. 2000), of the ESO Very Large Telescope (VLT), on the nights of March

30 (UT) and April 2, 2003 under good seeing ($0''.9$ - $0''.7$) conditions. Four 30 minutes exposures and two 1 hour exposures were secured on the first and fourth night after the burst, respectively, using two different beam splitters (dichroic #1 and #2). Two UVES standard settings were used, the so-called DIC1 (R346 nm, B580 nm), and the DIC2 (R437 nm, B860 nm). This combination allowed us to get on the first observing date two spectra covering the full optical range (303-1060 nm), except for small gaps near 575 and 855 nm, and one similar spectrum on the second night. The use of a $0''.8$ slit width provides a resolving power of $\lambda/\Delta\lambda \sim 55,000$ or 5.5 km/s (FWHM). The slit was oriented along the parallactic angle in order to minimize losses due to the atmospheric dispersion.

The raw data were reduced using the UVES pipeline (v1.4) implemented in the ESO-MIDAS software package (Ballester et al. 2000). This pipeline reduction includes flat-fielding, bias and sky subtraction and a relative wavelength calibration which has an accuracy of ± 0.5 km/s. The optimum extraction method has been used, which assumes a Gaussian profile for the cross-dispersion flux distribution and is optimized for low SNR spectra. The individual reduced spectra were also corrected for the airmass, the atmospheric absorption bands could however not be removed because of saturation. No correction for vacuum wavelengths or heliocentric velocities (-16.23 and -17.36 km/s for the two nights respectively) was done for the final spectra, this was taken into account later for the redshift determination (see Sec. 4).

We also did an absolute flux calibration using the master response curves determined by the ESO Garching Quality Control² (see also Hanuschik 2003). Comparison with photometric data of the afterglow from the literature (Matheson et al. 2003) showed that the continuum of the flux calibrated spectrum was almost a factor 2 too low. This can hardly be explained with bad seeing. It seems, however, to be a common problem in UVES flux calibration. Comparison with FORS spectra taken at the same time suggest that the UVES flux calibration is about a factor of 1.6 too low (Wiersema et al. 2006). We therefore recalibrated the spectrum using photometric data from Matheson et al. (2003), obtained at the same time as our spectroscopic observations.

The log of the observations are noted in Table 1. As an example, the entire reduced spectrum of the third epoch is shown in Fig. 1.

3. LINE ANALYSIS

3.1. Emission lines

We detected a range of emission lines from the GRB host galaxy. The Balmer series down to H δ , the forbidden lines [OII] $\lambda\lambda 3727, 3729$ and [OIII] $\lambda 5007$ as well as [Ne III] $\lambda 3869$ could be identified. H α was also detected though it lies in the middle of the atmospheric A absorption band. Fortunately, it fell between two of the resolved atmospheric absorption lines in the atmospheric A band and is therefore very little affected by absorption (see Fig. 2). H δ and H γ could only be

² http://www.eso.org/observing/dfo/quality/UVES/qc_std_qc1.html#response

TABLE 1
LOG OF THE OBSERVATIONS

epoch	date	UT	d after GRB	exp. [min]	R mag	seeing ["]	airmass	wavelength range [nm]
1	30/3/2003	03:22:44	0.6556	30	15.27	0.73	1.45	303-388 + 476-684
		03:55:43	0.6785	30	15.31	1.03	1.49	373-499 + 660-1060
2	30/3/2003	04:29:01	0.7016	30	15.38	0.97	1.59	303-388 + 476-684
		05:01:53	0.7244	30	15.46	0.75	1.74	373-499 + 660-1060
3	02/4/2003	00:46:54	3.5474	60	17.24	0.49	1.72	383-499 + 660-1060
		01:51:51	3.5925	60	17.25	0.72	1.49	303-388 + 476-684

NOTE. — Dates given are the start of the observations

detected clearly in the data from the third epoch. Of the two [OIII] lines at 4963 Å and 5007 Å, the 4963 Å line unfortunately falls in the gap of the detector in the red arm which consists of a mosaic of two chips. [N II] λ 6586 was not detected, but a reliable 2σ upper limit could be derived because of the high resolution, despite the fact that this region in the spectrum was also affected by atmospheric absorption bands.

The [OII] doublet was well resolved in the spectra of the fourth night (see Fig. 2) which was only possible in three other bursts, GRB 990506 and GRB 000418 Bloom et al. (2003) as well as GRB 060218 (Wiersema et al. 2006). This is especially interesting because the [OII] $\lambda\lambda$ 3727/3729 ratio allows the determination of the electron density n_e (Osterbrock 1989). In our spectrum, the ratio of the two lines is 0.53 ± 0.10 for the third epoch when the S/N was high enough to resolve the 3727 Å-line, because the afterglow continuum had faded away. This ratio is consistent with the lower value of 0.66 for $n_e \rightarrow 0$. Similar ratios were found for the hosts of GRB 990506, GRB 000418 and GRB 060218 with values of 0.57 ± 0.14 , 0.75 ± 0.11 and 0.62 ± 0.05 respectively. To measure the emission line fluxes, we fitted the lines with a Gaussian and compared it with measuring the line flux directly which gave similar results. The properties of the emission lines in the individual spectra as well as the mean value of the flux from first night's spectra are listed in Table 2. The flux of the emission lines is generally higher in the two spectra from the first night (epoch 1 and 2) which could be due to different seeing and it also varies between the two exposures. As the light curve of the first night showed large variations and even small color changes (Matheson et al. 2003; Lipkin et al. 2004), this might also affect the spectrum. Therefore, we take the emission line fluxes from the 3rd epoch for further calculations as the continuum might be less influenced by intrinsic changes of the afterglow spectrum.

Even after recalibrating the spectra with photometric data, our emission line fluxes are a factor of 1.3 (second epoch) to 1.4 (first epoch) lower than the values found by Gorosabel et al. (2005), Sollerman et al. (2005) in late FORS spectra from the host galaxy. As they used a 1''.0 slit and a fixed orientation angle covering most of the galaxy, these data might not be entirely comparable to our spectra, though the line ratios are very similar to those found from later spectra.

3.2. Absorption lines

Compared to other bursts from which spectra could be obtained, GRB 030329 has a very low redshift. Therefore, most of the metal absorption lines are still far in the UV, outside the detection range of UVES.

However, we detect the Mg II $\lambda\lambda$ 2797, 2803 doublet clearly resolved as well as Mg I λ 2852, which all reveal to have several well resolved velocity components. Voigt profiles were fitted to these absorption features using the FIT/LYMAN package (Fontana & Ballester 1995) in MIDAS and the column densities determined for each component (see Sec. 5)

Interstellar NaD λ 5890 and Ca II λ 3933 from our Galaxy were also detected and resolved in three different clouds, which allows an independent determination of the Galactic extinction. These two elements do usually not occur in the same regions in the galaxy and their wavelength and properties can therefore be different. We find that the first two clouds have the same shift within the accuracy, the third one however has a different position for NaD and Ca II. The FWHM and the ratio of the EWs NaD/Ca II are also different within each cloud which favors different states of the ISM for the origin of the two absorption lines (Welty et al. 1996).

We could, however, not detect any NaD λ 5890, Ca II λ 3933 or Ti II λ 3242 absorption from the host galaxy, whereas the ratio of Ca II to Mg I, which have similar ionization potentials, found in GRB 020813 (Savaglio & Fall 2004) was around 1. Ratios found in the MW can vary between 0.01 and 1 depending on the properties of the ISM (Welty et al. 1999)

The properties of the absorption lines are listed in Table 3.

4. RESULTS

4.1. Redshift

The redshift of the host galaxy was determined from the [O III] λ 5007, H α and H β emission lines of the first epoch (Greiner et al. 2003a) as $z = 0.1685$. We did a refined analysis using the emission lines [O II] $\lambda\lambda$ 3726, 3729, [O III] λ 5007, H α and H β , corrected for heliocentric velocities of -16.23 and -17.36 km/s for night 1 and 4 respectively. From this, we derive a value of $z = 0.16867 \pm 0.00001$, consistent with the value found by Matheson et al. (2003) and Sollerman et al. (2005). Note, however that this is the mean redshift of the GRB host galaxy, not of the GRB itself.

4.2. Broadening of the emission lines

Low resolution spectra are usually not able to distinguish between instrumental resolution and intrinsic

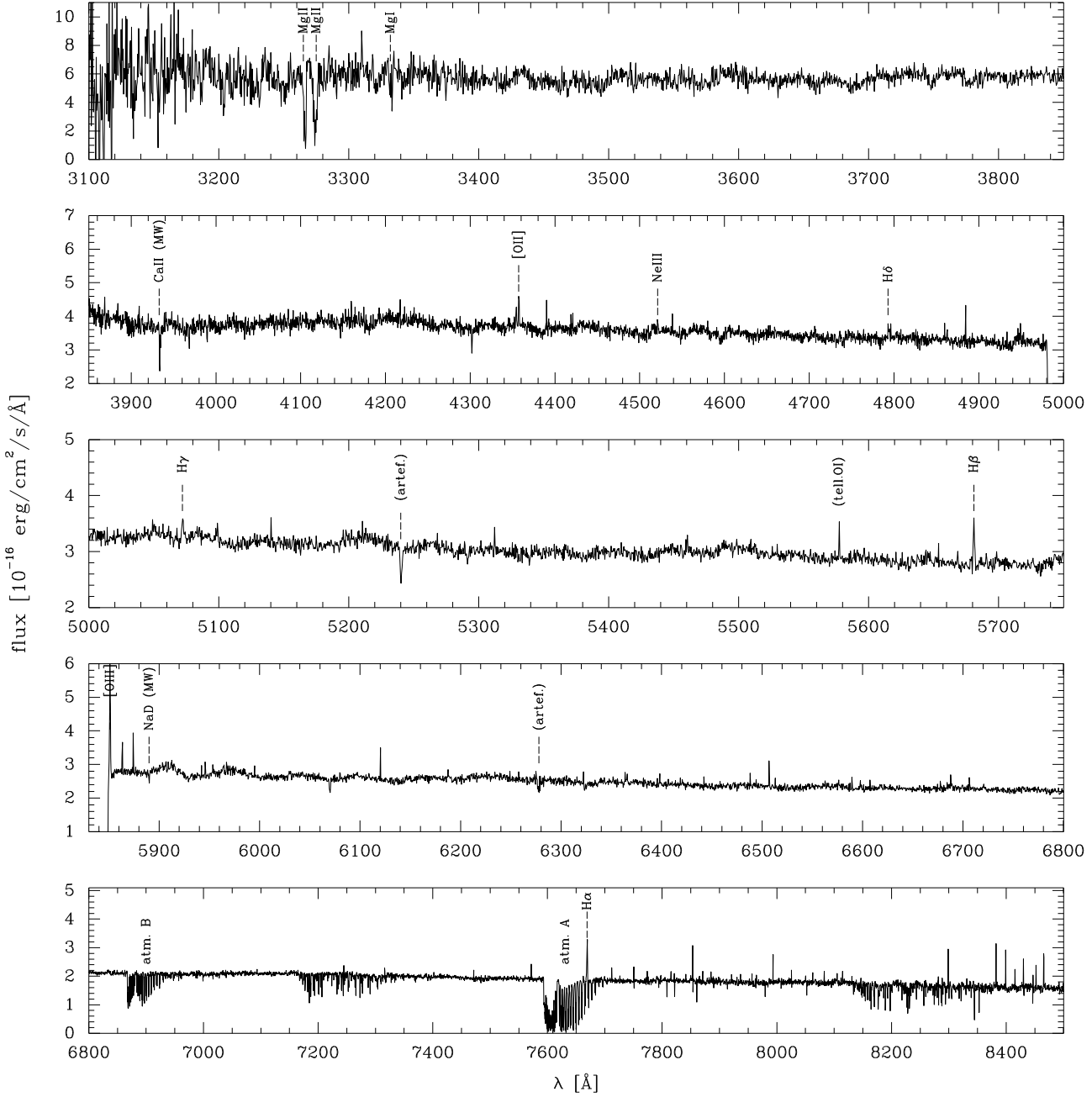


FIG. 1.— Total UVES spectrum of the fourth night after the burst where the afterglow continuum has faded away enough to result in a good S/N of the host emission lines. For better visualization of the spectral lines in this graph, the spectra have been smoothed and rebinned to 0.4 \AA . Ca II and NaD lines are from absorption in the Milky Way (MW), all other absorption and emission lines are from the host galaxy at $z=0.16867$. The emission features not marked in panel 3 and 4 are due to imperfect atmospheric emission line removal as their FWHM is much smaller than from the lines of the host galaxy and they are only visible in the spectra of this epoch. The two features at 5238 and 6069 Å are due to bad pixels on the CCD. Note that the scale of the y-axis changes for the different panels.

broadening of the host emission lines due to galaxy rotation and turbulence of the medium.

From our high resolution spectra (FWHM=5.5 km/s), we find that all emission lines in our spectra are clearly broadened compared to the resolution of the instrument. The FWHM of the emission lines lies between 35 and 55 km/s, restframe corrected. This fits well to the fact that the host of GRB 030329 is a dwarf galaxy, which have typical radial velocities up to 100 km/s. We might however not see the whole rotational velocity spread if the galaxy is not seen edge on.

4.3. Galactic and host extinction

For the determination of the Galactic extinction, usually sky catalogs such as Schlegel et al. (1998) or Dickey & Lockman (1990) are used. The strength of interstellar lines like NaD $\lambda 5890$ however allows a different and more accurate determination of the extinction using e.g. the model of Munari & Zwitter (1997). In our spectra, Galactic NaD as well as Ca II show a triple absorption peak, indicating three clouds in our Galaxy in the line of sight. The NaD-line gives an extinction of $E_{B-V} = 0.013 \pm 0.004, 0.007 \pm 0.002$ and

TABLE 2
EMISSION LINE CHARACTERISTICS

Line	epoch	λ_{rest} [Å]	λ_{obs} [Å]	FWHM [Å] and [km/s]	Flux (measured) [10^{-17} erg/cm ² /s/Å]	Flux (A _V corr.) [10^{-17} erg/cm ² /s/Å]	Mean(1,2) A _V corr. [10^{-17} erg/cm ² /s/Å]
OII	1	3726	(4354)	(0.9)	$<17.3 \pm 0.5$	$<32.1 \pm 0.9$	< 35.2
	2		(4354)	(0.9)	$<20.6 \pm 0.5$	$<38.2 \pm 0.9$	
	3		4354.29	0.91 ± 0.10 64 \pm 7	4.81 \pm 0.5	8.92 \pm 0.9	
OII	1	3728	4357.67	0.62 ± 0.10 37 \pm 7	11.5 \pm 0.5	21.4 \pm 1.0	27.3
	2		4357.37	0.69 ± 0.10 40 \pm 7	17.9 \pm 0.5	33.3 \pm 1.0	
	3		4357.43	0.96 ± 0.10 56 \pm 7	9.04 \pm 0.5	16.7 \pm 1.0	
NeIII	1	3869	4520.80	0.74 ± 0.10 42 \pm 6	6.6 \pm 2.0	12.1 \pm 3.7	13.85
	2		4521.39	0.50 ± 0.10 28 \pm 6	8.5 \pm 2.0	15.6 \pm 3.7	
	3		4521.27	0.91 ± 0.10 51 \pm 6	3.4 \pm 2.0	6.24 \pm 0.9	
H δ	1	4101	(4793)	(0.9)	$<16.3 \pm 1.0$	$<29.2 \pm 1.8$	< 30.1
	2		(4793)	(0.9)	$<17.3 \pm 1.0$	$<31.0 \pm 1.8$	
	3		4793.07	0.83 ± 0.10 45 \pm 6	3.35 \pm 1.5	6.00 \pm 1.8	
H γ	1	4340	(5072)	(0.9)	$<8.39 \pm 1.0$	$<14.6 \pm 1.8$	<16.9
	2		(5072)	(0.9)	$<11.0 \pm 1.0$	$<19.2 \pm 1.8$	
	3		5072.21	0.81 ± 0.10 41 \pm 6	3.2 \pm 1.5	5.58 \pm 1.8	
H β	1	4861	5681.17	0.90 ± 0.10 41 \pm 5	10.0 \pm 1.0	16.3 \pm 3.2	15.1
	2		5680.86	0.95 ± 0.10 43 \pm 5	8.4 \pm 1.0	13.8 \pm 3.2	
	3		5680.99	1.00 ± 0.10 45 \pm 5	7.8 \pm 0.5	12.8 \pm 1.7	
OIII	1	5007	5850.90	0.77 ± 0.10 33 \pm 5	39.4 \pm 0.5	63.4 \pm 0.8	62.3
	2		5851.01	0.81 ± 0.10 36 \pm 5	38.0 \pm 0.5	61.1 \pm 0.8	
	3		5851.03	0.76 ± 0.10 33 \pm 5	31.8 \pm 0.5	51.2 \pm 0.8	
H α	1	6563	7669.24	1.33 ± 0.10 45 \pm 4	23.5 \pm 1.0	32.9 \pm 1.3	35.3
	2		7669.22	1.21 ± 0.10 40 \pm 4	26.9 \pm 1.0	37.6 \pm 1.3	
	3		7669.29	1.40 ± 0.10 47 \pm 4	21.3 \pm 0.5	29.8 \pm 0.8	
N II	1	6586	(7695)	(1.20)	$<8.77 \pm 1.0$	$<12.2 \pm 1.3$	<12.8
	2		(7695)	(1.20)	$<9.63 \pm 1.0$	$<13.4 \pm 1.3$	
	3		(7695)	(1.20)	$<2.67 \pm 0.5$	$<3.71 \pm 0.8$	

NOTE. — Values for the emission lines for the three different datasets with the numbers indicating the spectra taken in the first and the fourth night after the burst as described in Table 1. The measured wavelenghts are in air and not corrected for heliocentric velocity, FWHM is restframe corrected. Fluxes are given as the measure value and the value corrected for Galactic and host extinction as described in Sec. 4.3

0.002 ± 0.001 for the three clouds respectively which results in a total extinction of $E_{B-V} = 0.022 \pm 0.005$ or $A_V = 0.068$ as $A_V = R_V E_{B-V}$ with $R_V = 3.1$ for a MW extinction law (Cardelli et al. 1989). This is comparable to the extinction determined from the Schlegel sky catalog of $E_{B-V} = 0.025$.

The extinction in the host galaxy can in principle be derived from the Balmer line decrement, the constant flux ratio of the Balmer lines derived from line transition properties, with unextinguished values of $H\alpha/H\beta = 2.76$ and $H\gamma/H\beta = 0.474$ for a temperature of 10,000 K and case B recombination (Osterbrock 1989). From our spectrum we obtain $H\alpha/H\beta = 2.73 \pm 0.2$ which is consistent with no extinction. The ratio $H\gamma/H\beta = 0.41 \pm 0.15$ would give an extinction of $E(B-V) = 0.74 \pm 0.7$ which is unfortunately quite inaccurate due to the relatively large error in the emission line fluxes. In addition, the Balmer lines can be affected by absorption from an underlying stellar population depending on the age of the galaxy. This affects $H\beta$ and $H\gamma$ much more than $H\alpha$, which means that the derived extinction should be seen as an upper limit. However, in the UVES spectra, we could not identify any underlying stellar absorption, whereas Gorosabel et al. (2005) derive a relatively high correction, comparable to the value of the fluxes for $H\gamma$ and $H\delta$ from their stellar population models. We consider it therefore to be more appropriate to use an extinction value derived from

the broad band afterglow as it was done in Kann et al. (2006). They derive a value of $A_V = 0.39 \pm 0.15$, fitting an SMC extinction law, which differs however very little from the fit with a MW extinction law.

To correct the emission line fluxes, we then use $A_V = 0.39$ for the host extinction and $A_V = 0.068$ for the Galactic extinction applying a MW extinction law (see Table2).

4.4. SFR

A direct indicator of the current SFR in a galaxy is the flux from nebular emission lines such as $H\alpha$ that had been ionized by young, massive stars. Using the $H\alpha$ flux from the 3rd epoch, which is corrected for extinction but not for a possible underlying stellar absorption, we derive a SFR of the host galaxy according to Kennicutt et al. (1998) of $SFR [M_\odot/yr] = 7.9 \cdot 10^{-42} 4\pi f_{H\alpha} d_L^2 = 0.198 \pm 0.006 M_\odot/yr$ which is consistent with the value in Hjorth et al. (2003) of $SFR_{H\alpha} = 0.17 M_\odot/yr$ from the FORS spectra. Another indicator for the SFR are forbidden lines like [OII] with the drawback of being only indirectly coupled to the ionizing flux of young stars but very sensitive to the ionization state of the ISM. For [OII], the corresponding equation $SFR [M_\odot/yr] = 1.4 \cdot 10^{-41} 4\pi f_{[OII]} d_L^2$ gives a value of $0.302 \pm 0.006 M_\odot/yr$ which is higher than the value derived from $H\alpha$. As the SFR from [OII] seems to

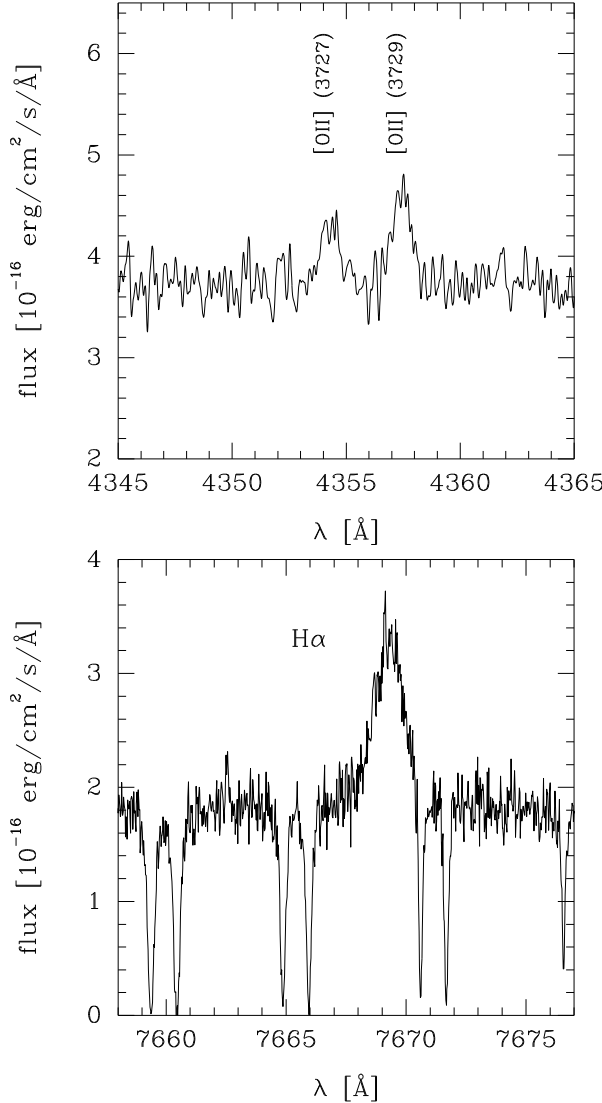


FIG. 2.— Upper figure: Resolved OII lines in the spectra from the 3rd epoch. For better visualization, the spectrum has been smoothed with a box car width of 10 pixels. Lower figure: Position of the H α line in between two atmospheric absorption lines.

be less reliable, we adopt here the SFR from H α . A SFR of $0.198 M_{\odot}/\text{yr}$ is not very high compared to other galaxies at this redshift, but one has to consider the low mass of the host galaxy as already noted in Sollerman et al. (2005). Savaglio, Glazebrook and Le Borgne (2006, in prep.) derive a low total stellar mass for the host of $M_{\star} = 10^{7.75 \pm 0.15} M_{\odot}$. This gives a specific SFR (SSFR) per unit mass of $\log \text{SFR}/M = -8.5 \text{ yr}^{-1}$. Furthermore, the host galaxy of GRB 030329 is underluminous with an absolute magnitude of $m_V = -16.37$ (Fruchter et al. 2006). This can be used to scale the SFR with the luminosity fraction compared to a standard galaxy with $m_V(\text{abs}) = -21$ to derive the SFR/L (Christensen et al. 2004). For our galaxy, we get a value for the SFR/L of $14.1 M_{\odot} \text{ yr}^{-1} L_{*}^{-1}$ which is high compared to the average of other host galaxies of $9.7 M_{\odot} \text{ yr}^{-1} L_{*}^{-1}$ as found by Christensen et al. (2004).

4.5. Metallicity of the host

TABLE 3
ABSORPTION LINE CHARACTERISTICS

Line	epoch	λ_{rest} [Å]	λ_{obs} [Å]	FWHM [Å]	EW [Å]
Mg II	1	2796	3266.1	1.7 ± 0.1	1.3 ± 0.1
	2		3266.2	1.8 ± 0.2	1.3 ± 0.2
	3		3266.7	1.9 ± 0.2	1.1 ± 0.2
Mg II	1	2803	3274.5	1.9 ± 0.1	1.3 ± 0.2
	2		3274.7	1.4 ± 0.2	0.9 ± 0.2
	3		3274.8	2.8 ± 0.2	1.63 ± 0.30
Mg I	1	2852	3332.5	1.2 ± 0.2	0.25 ± 0.18
	2		3333.0	1.3 ± 0.2	0.25 ± 0.18
	3		3332.9	1.9 ± 0.2	0.39 ± 0.25
NaD	1	5890	5889.58	0.23 ± 0.02	0.053 ± 0.01
			5890.27	0.24 ± 0.05	0.028 ± 0.01
			5890.60	0.16 ± 0.05	0.006 ± 0.01
			5889.64	0.28 ± 0.05	0.050 ± 0.01
			5890.21	0.25 ± 0.05	0.027 ± 0.01
			5890.54	0.17 ± 0.05	0.009 ± 0.01
			5889.64	0.21 ± 0.05	0.031 ± 0.01
			5890.01	0.10 ± 0.05	0.021 ± 0.01
			5890.15	0.05 ± 0.05	0.013 ± 0.01
Ca II	1	3933	3933.5	0.25 ± 0.03	0.16 ± 0.01
			3933.9	0.22 ± 0.03	0.05 ± 0.01
			3934.6	0.30 ± 0.03	0.04 ± 0.01
			3933.5	0.23 ± 0.05	0.18 ± 0.01
			3933.9	0.17 ± 0.05	0.03 ± 0.01
			3934.5	0.28 ± 0.05	0.06 ± 0.01
			3933.5	0.27 ± 0.05	0.23 ± 0.01
			3933.9	0.13 ± 0.05	0.03 ± 0.01
			3934.5	0.30 ± 0.05	0.09 ± 0.01

NOTE. — The upper part are absorption lines from the host galaxy, the lower part from the MW. The FWHM of the Mg lines are the widths over the rebinned lines. The different wavelengths and EWs of the NaD interstellar lines from the third epoch are due to imperfect sky line removal from telluric NaD emission.

There are a number of secondary, empirical metallicity calibrators derived from the abundances of nebular emission lines. The most frequently used, because easiest to get, is the $R_{23} = \frac{f_{[\text{OIII}]\lambda 3727} + f_{[\text{OIII}]\lambda 4959,5007}}{f_{\text{H}\beta}}$ parameter (Kobulnicky et al. 1999). $[\text{O III}]\lambda 4959$ was not detected due to the gap in the spectrum, there is, however a fixed ratio between the two $[\text{O III}]$ lines, $f_{[\text{OIII}]\lambda 5007} = 3 \cdot f_{[\text{OIII}]\lambda 4959}$.

The R_{23} parameter gives two possible solutions, in our case either a metallicity of $12 + \log(\text{O/H}) = 7.8$ or 8.7. This degeneracy can be broken using the $[\text{N II}]\lambda 6586$ to H α ratio (Lilly et al. 2003). As noted in Sollerman et al. (2005), no $[\text{N II}]$ was detected in the spectra of GRB 030329, except from the FORS spectrum of May 1st (Hjorth et al. 2003), which seems to be spurious. Due to the high resolution of the UVES spectrum however, we were able to put a strong 2σ upper limit of $[\text{N II}]$ (see Table 2) and therefore to derive a ratio of $[\text{N II}]/\text{H}\alpha$ from the strongest upper limit at the 3rd epoch of $< 0.12 \pm 0.02$. This favors a lower branch solution according to Lilly et al. (2003), which gives a low metallicity value of $12 + \log(\text{O/H}) = 7.8$ or $1/7 Z_{\odot}$, assuming $12 + \log(\text{O/H}) = 8.66$ for solar metallicity (Asplund et al. 2004). The low mass of the host galaxy supports a low value for the metallicity.

The R_{23} parameter however has turned out to be affected by systematic errors for high and low metallicities (Bresolin et al. 2004). Wiersema et al. (2006) showed

that the metallicity of the GRB 060218 host, derived from the oxygen abundances, is $12 + \log(\text{O/H}) = 7.54$, compared to 8.0 from the R_{23} parameter. For a direct calibration from the abundances however, the electron temperature and density have to be known which rely on the detection of $[\text{OIII}] \lambda 4363$ and the detection or low error flux measurements of the $[\text{OII}] \lambda\lambda 3727, 3729$ or $[\text{SII}] \lambda\lambda 6716, 6731$ doublets, which were not detected for the GRB 030329 host or only with large errors in the case of $[\text{OII}]$.

5. ABSORPTION LINE KINEMATICS

5.1. *Fitting of the absorption systems*

For the absorption lines in the host galaxy, we found seven different velocity components for the two lines of the Mg II doublet, whereas Mg I only shows six because of its lower line strength. The components span a velocity range of about 260 km/s (see Fig. 3) in both Mg II and Mg I. Mg I shows nearly the same velocity differences as the Mg II components, so it seems that both arise from the same structure. This does not necessarily have to be the case due to the different ionization stages. The fit for the first two clouds however, does not match very well the Mg I components, which might point to a different spatial origin for this component. The b parameter of the seven components is in the range of 5–11 km/s which is relatively narrow compared to QSO-Mg absorbers with similar EWs (Churchill et al. 2003).

No time variability of the absorption lines was seen between the different epochs and we therefore only used the first epoch for the fitting due to the better S/N for the absorption lines. This rules out an origin in the vicinity of the burst (Perna & Loeb 1998; Prochaska et al. 2006), where one would expect a considerable weakening of the Mg absorption between the first and the fourth night. Furthermore, the Mg II absorption in 5 of the 7 components goes down to zero, supporting the suggestion that the absorption does not occur at a very short distance from the central source. Otherwise, scattered light could lead to a covering factor smaller than one (Savaglio & Fall 2004).

The individual components at the different velocity shifts have similar column densities, though comparison of the ratios $N(\text{Mg II})$ to $N(\text{Mg I})$ show that the conditions in the different absorbing structures might vary slightly. The total Mg II column density is $10^{14.1 \pm 0.1} \text{ cm}^{-2}$ which is in the regime of DLAs (Rao & Turnshek 2000). The gas in DLAs is predominantly neutral which is supported for our GRB by the presence of a relatively large column density of Mg I ($10^{12.3 \pm 0.1} \text{ cm}^{-2}$) compared to $N(\text{Mg II})$. This ratio is also higher than in QSO-Mg absorbers (Churchill et al. 2003).

5.2. *Interpretation of the Mg I & II velocity structure*

Mg I and II have been detected in many GRB afterglow spectra (Castro et al. 2000; Fiore et al. 2005; Starling et al. 2005; Penprase et al. 2006), where two types of velocity spreads were found. The first type shows saturated Mg lines with a velocity broadening up to 200 km/s, comparable to the instrumental resolution in low resolution spectra or resolved in high

resolution spectra as a truly broad absorption feature as in Penprase et al. (2006). The broad features from low resolution spectra could sometimes be partially resolved as in Castro et al. (2000), who found a second component with a Δv of 180 km/s. Therefore, it is likely that the broad lines sometimes actually consist of several distinct components, which could have been resolved with higher resolution spectrographs. The other type shows many high velocity components with Δv up to 3000 km/s as in Fiore et al. (2005) and Starling et al. (2005).

The high velocity components are usually explained as being connected to the GRB itself like tracing nebula shells from former mass losses of the progenitor star, excited by the GRB (Mirabal et al. 2002) or strong winds which blow material of the star away from the Wolf-Rayet progenitor. The latter scenario was suggested for the high velocity components in GRB 021004 (Starling et al. 2005; Fiore et al. 2005; Chen et al. 2005). They found both broad and narrow structures in all the strongest absorption lines in UVES spectra of GRB 021004 and GRB 020813 up to velocities of 3000 km/s. The velocities measured in GRB 030329, however, are much lower, such winds can therefore not be the explanation for the components seen in our spectra. If those high velocity features were common for GRBs, they should have also been detected in GRB 030329, in addition to the low velocity components, but there are no absorption features visible at comparable velocity distance from the main component. Neither were they detected in any other spectra than those of GRB 021004, GRB 020813 and recently GRB 050505 (Berger et al. 2005) and GRB 051111 (Penprase et al. 2006), though the distances are far enough to be resolved in low resolution spectra as in the case of GRB 021004 (Mirabal et al. 2002). Either the ISM around the burst must be quite dense to produce these clumps, not all GRB progenitors have high mass losses and strong winds or the reason for these components is something completely different.

In some recent bursts, fine-structure lines of Si II, Fe II, C II and C IV could be detected as first reported by Vreeswijk et al. (2004) in a GRB spectrum. Fine-structure lines have only been found in high density environments such as η Carinae (Gull et al. 2005). It is assumed that in GRBs, these lines come from electron excitation in the hot, turbulent vicinity of the burst. They are however not the reason for the structures in the Mg lines in our spectrum as these transitions are extremely weak for Mg (Morton 2003).

Another possibility for the origin of the Mg lines in the spectrum of the GRB 030329 afterglow are supergalactic winds from starburst regions as found in spectra of low-redshift starburst galaxies and clearly visible e.g. in $\text{H}\alpha$ light from M82. These winds were discovered in X-ray data, as the heated ISM emits X-rays. Heckman et al. (2000) studied the structures of NaD lines from such starburst galaxies. They found blueshifted components relative to the host galaxy up to 600 km/s with Doppler width of more than 100 km/s which seems likely for a hot environment ($T \approx 70,000$ K). This however rules out the possibility of an active starburst wind for our absorption line features as the velocities are too low for a wind origin and in addition, the lines are very narrow, so the absorbing atoms cannot be in a hot environment.

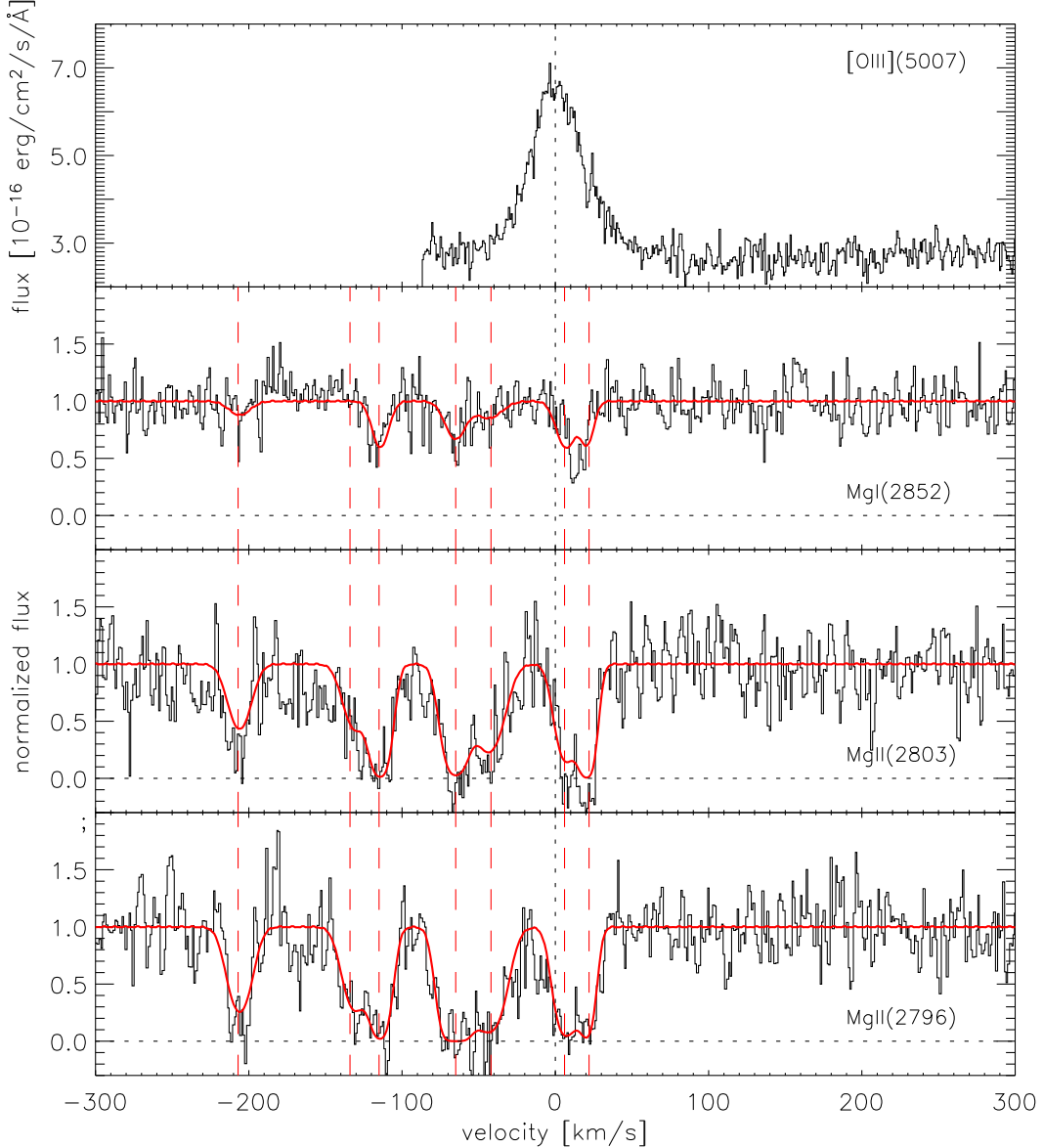


FIG. 3.— Velocity distribution of the seven components in the Mg II-doublet and six in Mg I and the corresponding fit to the different components with FIT/LYMAN. $v=0$ km/s corresponds to the redshift determined by the emission lines from the host. We used only the first sample of the first night as this had the highest continuum and therefore the best statistics for the absorption lines. There was also no change visible in the fits from the other samples.

TABLE 4
DIFFERENT COMPONENTS IN THE HOST ABSORPTION LINES

Component	MgII[2796]		MgII[2803]		MgI[2852]		N(MgII)/N(MgI)
	b [km/s]	log N [cm ⁻²]	b [km/s]	log N [cm ⁻²]	b [km/s]	log N [cm ⁻²]	
v ₁ = +22 km/s	4.7±0.8	12.91±0.26	4.7±0.8	13.50±0.24	4.7±0.8	11.53±0.13	2.07
v ₂ = +6 km/s	7.7±0.9	13.01±0.11	7.7±0.9	13.10±0.07	7.7±0.9	11.75±0.09	1.61
v ₃ = -42 km/s	11.1±1.4	13.06±0.07	11.1±1.4	13.13±0.06	11.1±1.4	11.38±0.18	2.02
v ₄ = -65 km/s	8.3±1.2	13.53±0.29	8.3±1.2	13.41±0.10	8.3±1.2	11.66±0.10	2.12
v ₅ = -115 km/s	6.4±0.9	13.06±0.18	6.4±0.9	13.42±0.20	6.4±0.9	11.68±0.10	1.90
v ₆ = -134 km/s	9.1±1.3	12.70±0.06	9.1±1.3	12.81±0.08	...	<6.5	>6.6
v ₇ = -207 km/s	9.0	12.71±0.05	9.0	12.80	9.0	11.20±0.23	1.86

NOTE. — Values with no error bars indicate that they had to be fixed in order to achieve a reasonable fit.

These winds might however not be the end of the story. In the MW as well as in other galaxies, so-called “high velocity clouds have been found, consisting mainly of HI, but OVI has also been discovered from the same region (Fox et al. 2005). This gave rise to the theory of the galactic fountain where starburst regions blow hot, ionized material out into the halo which then cools down and eventually falls back again onto the galaxy. The Mg absorption lines in our spectra might therefore be caused by some intermediate stages of that process, when the starburst wind has cooled and slowed down. The fact that, except for the two lowest-velocity systems, the velocities are larger than the rotational velocity of the host galaxy as determined from the emission line width, indicates that they are most likely not just related to large structures in the host galaxy like spiral arms. With the escape velocity typically being less than 50% larger than the mean rotational velocity, half of our velocity systems are likely to be unbound to the gravitational potential of the host galaxy. The star burst wind suggestion is therefore an appealing scenario for those structures.

The same process might cause Mg II absorbers, which have often been found in the sightline of QSOs (Ellison et al. 2003) with large EW. Similar structures have also been discovered in Lyman break galaxies (LBG) (Adelberger et al. 2003) but only for C IV absorption lines. DLAs associated with Mg-absorbers show black bottom saturated Mg velocity components with narrow spreads of about 40 to 60 km/s. So-called “doubles have smaller EWs and highly complex features separated by a large Δv (Churchill et al. 1999) with their individual components having Doppler widths comparable to those found in GRB 030329. This might lead to the conclusion that Mg QSO absorbers and GRB absorbers have the same origin but that they are probing different regions of the galaxy. Petitjean (2005) also suggested that QSO-Mg absorbers could arise in optically thick clouds in the galactic halos, created by material ejection from starburst regions, being the remnants of a former starburst wind.

For strong QSO absorbers, there usually exist velocities red- and blueshifted compared to the central redshift of the intervening galaxy (Bond et al. 2001) whereas in our case mainly blueshifted lines exist, except for the first two components. This might be a hint to the position of the burst in the galaxy. If these components are really due to some metal rich clouds in or around the host galaxy, the burst could lie slightly behind the center plane of the galaxy or the star burst cloud which causes the few redshifted components, whereas the rest of the lines come from material flowing away from the burst

site.

6. CONCLUSION

In this paper, we have presented high resolution spectra of a typical long-duration GRB at $z=0.16867$, which had the rare case to contain both emission lines from the host galaxy as well as absorption lines from the surrounding medium of the burst. The host galaxy is a sub-luminous ($m_V=-16.37$), low mass ($M_\star = 10^{7.75 \pm 0.15} M_\odot$) starburst with a high SFR/L of $14.1 M_\odot \text{ yr}^{-1} L_\star^{-1}$ or $\log \text{SFR}/M = -8.5 \text{ yr}^{-1}$ compared to other galaxies at this redshift. This confirms the values of the SSFR found by Hjorth et al. (2003) and Sollerman et al. (2005) from late FORS spectra of the host galaxy. Furthermore, the high resolution UVES spectra made it possible to derive a strong upper limit for [N II] and therefore to place the value of the metallicity in the lower branch with $\log(\text{O/H})=7.8$ or $1/7 Z_\odot$.

In absorption, only Mg II and Mg I from the host could be detected. Due to the high resolution again, however, we were the first to resolve these usually broad absorption lines into six and seven narrow velocity components for Mg I and Mg II respectively. These components span a relatively small range of velocities up to $v \sim 260 \text{ km/s}$, which can usually not be resolved in low resolution spectra. The majority of these components are however outside of the galaxy whose emission lines have only a width of 55 km/s. Both Mg I and Mg II seem to originate in the same clouds which are predominantly neutral with $N(\text{Mg II})/N(\text{Mg I})$ of around 2. Structures similar in width and velocity distance have been found in QSO Mg absorbers. They could be clouds in the halo of the host galaxy, possibly from material ejected from the inner regions of the galaxy by former starburst driven superwinds which have already slowed down.

The *Swift* satellite now provides faster information of the burst position and more early, high resolution spectra can be obtained. Very early spectra, compared with later times, could also reveal possible changes of the absorption lines due to ionization of the ISM by the burst (Vreeswijk et al. 2006b).

C.T. wants to thank Johan Fynbo for reading the manuscript and discussions about upper limits as well as Alexander Kann for editing the text and the references. Thanks also to Klaas Wiersema for the preprint of his paper on 060218 and informations about advanced line diagnostics. The “DARK Cosmology Centre is funded by the Danish National Research Foundation

REFERENCES

Adelberger, K. L., Steidel, C. C., Shapley, A. E., & Pettini, M. 2003, ApJ584, 45

Asplund, M., Grevesse, N., Sauval, A. J., Allende Prieto, C. and Kiselman, D. 2004, A&A417, 751

Ballester, P., Dorigo, D., Disarò, A. Pizarro de La Iglesia, J. A., & Modigliani, A. 2000, Astronomical Data Analysis Software and Systems IX, ASP Conference Proceedings, Vol. 216

Barth, A. J. et al. 2003, ApJ584, L47

Berger, E., et al., ApJ642, 979

Bloom, J. S., et al. 2003, AJ, 125, 999

Bond, N. A., Churchill, C. W., & Charlton, J. C. 2001, ApJ562, 641

Bresolin, F., Garnett, D. R. and Kennicutt, R. C., Jr. 2004, ApJ615, 228

Butler, N. et al. 2005, ApJ, 627, L9

Cardelli, J. A., Clayton, G. C., & Mathis, J. S. 1989, ApJ, 345, 245

Castro, S. et al. 2003, ApJ, 586, 128

Chen, H. W., Prochaska, J. X., Bloom, J. S., & Thompson, I. B. 2005, ApJ, 634, L25

Christensen, L., Hjorth, J., & Gorosabel, J. 2004, A&A, 425, 913

Churchill, C. W., Rigby, J. R., Charlton, J. C., & Vogt, S. S. 1999, ApJS, 120, 51

Churchill, C. W., Vogt, S. S. & Charlton, J. C. 2003, ApJ, 125, 98

Dekker, H., et al. 2000, *Proc. SPIE*, 4008, 534

Dickey, J. M., & Lockman, F. J. 1990, ARA&A, 28, 215

D'Elia, V. et al. 2005, GCN 4044

Ellison, S. L., Songaila, A., Schaye, J., & Pettini M., 2000, AJ, 120, 1175

Ellison, S. L., Mallén-Ornelas, G., & Sawicki, M. 2003 ApJ, 589, 709

Ellison, S. L., et al. 2006, MNRAS, 372, L38

Fiore, F. et al. 2005, ApJ, 624, 853

Fontana, E., & Ballester, P. 1995, ESO Messenger 80, 37

Fox A. J. et al. 2005, ApJ630,332

Fruchter, A. S., et al. 2006, Nature, 441, 463

Gehrels, N., et al. 2004, ApJ, 611, 1005

Gorosabel, J., et al. 2005, A&A, 444, 711

Greiner, J., et al. 2003, GCN 2020

Greiner, J., et al. 2003, Nature, 426, 157

Gull, T.R. et al. 2005, ApJ620, 442

Hanuschik, R. W. 2003, A&A, 407, 1157

Heckman, T. M., Lehnert, M. D., Strickland, D. K., & Armus, L., 2000, ApJS, 129, 493

Hjorth, J., et al. 2003, Nature, 423, 847

Kann, D. A., Klose, S., & Zeh, A. 2006, ApJ, 641, 933

Kennicutt, R. C. Jr., et al. 1998, ARA&A, 36, 189

Kobulnicky, H. A., Kennicutt R. C. Jr., & Pizagno, J. L. 1999, ApJ, 514, 544

Ledoux, C., Vreeswijk, P., Smette, A., Jaunsen, A. & Kaufer, A. 2006, GCN 5237

Lilly, S. J., Carollo, C. M., & Stockton, A. N. 2003, ApJ, 597, 730

Lipkin, Y. M., et al. 2004, ApJ, 606, 381

Masetti, N., et al. 2003, A&A, 404, 465

Matheson, T., et al. 2003, ApJ, 599, 394

Metzger, M. R., Djorgovski, S. G., & Kulkarni, S. R. 1997, Nature, 387, 878

Mirabal, N., et al. 2002, ApJ, 578, 818

Morton, D. C. 2003, ApJS, 149, 205

Munari, U., & Zwitter, T. 1997, A&A, 318, 269

Osterbrock, D. E. 1989, *Astrophysics of Gaseous Nebulae and Active Galactic Nuclei*, University Science Books, Mill Valley, CA

van Paradijs, J., et al. 1997, Nature, 386, 686

Petitjean, P., Aracil B., Srianand, R., & Ibata, R. 2000, A&A, 359, 457

Petitjean, P. 2005, Proceedings IAU Coll. 199

Penprase, B. E. et al. 2006, ApJ, 646, 358

Perna, R. & Loeb, A. 1998, ApJ, 501, 467

Peterson, B. A., & Price, P. A. 2003, GCN 1985

Prochaska, J. X., et al. 2005, GCN 3833

Prochaska, J. X., Chen, H.-W., & Bloom, J. S. 2006, ApJ, 648, 95

Prochter, G. E., Prochaska, J. X., & Burles, S. M. 2006, ApJ, 639, 766

Rao, S. M., & Turnshek, D. A. 2000, ApJS, 130, 1

Reichart, D. E., 1998 ApJ, 495, L99

Savaglio, S., & Fall, S. M. 2004, ApJ, 614, 293

Savaglio, S. 2006, NJP 8, 195

Schaye, J., Rauch, M., Sargent, W. L. W., & Kim, T.-S. 2000, ApJ, 541, L1

Schlegel, D. J., Finkbeiner, D. P., & Davis, M. 1998, ApJS, 80, 1

Sollerman, J., et al. 2005, New Astronomy, 11, 103

Stanek, K. Z., et al. 2003, ApJ, 591, L17

Starling, R. L. C., et al. 2005, MNRAS, 360, 305

Tripp, T. M., & Bowen, D. V. 2005, IAU Colloquium Proceedings No. 199

Vanderspek, R., et al. 2003, GCN 1997

Vreeswijk, P. M., et al. 2001, ApJ, 546, 672

Vreeswijk, P. M., et al. 2004, A&A, 357, 414

Vreeswijk, P. M. & Jaunsen, A. 2006, GCN 4974

Vreeswijk, P. M. et al. 2006, astro-ph/0611690

Welty, D. E., Morton, D. C., & Hobbes, L. M. 1996, ApJS, 106, 533

Welty, D. E., Frisch, P. C., Sonneborn, G. and York, D.G., 1999, ApJ, 512, 636

Wiersema, K., et al. 2006, A&A, submitted